Computers in Biology and Medicine 154 (2023) 106604

Contents lists available at ScienceDirect

Computers in Biology and Medicine

journal homepage: www.elsevier.com/locate/compbiomed

Performance assessment of electrode configurations for the estimation of omnipolar electrograms from high density arrays

Francisco Castells [a,*,1], Samuel Ruipérez-Campillo [a,b,f,*,1], Izan Segarra [a], Raquel Cervigón [c], Rubén Casado-Arroyo [d], José Luis Merino [e], José Millet [a]

[a] ITACA Institute, Universitat Politècnica de València, Valencia, Spain
[b] Department of Bioengineering, University of California, Berkeley, CA, USA
[c] Universidad de Castilla-La Mancha, Cuenca, Spain
[d] Cardiac Electrophysiology Lab, Hôpital Erasme, Brussels, Belgium
[e] Arrhythmia and Robotic Electrophysiology Unit, Hospital Universitario La Paz, Madrid, Spain
[f] School of Medicine, Stanford University, Palo Alto, CA, USA

ARTICLE INFO

Keywords:
High density electrode arrays
Omnipolar electrograms
Signal processing
Robust electrogram estimation
Electrophysiology
Biomedical engineering

ABSTRACT

Objective: The aim of this study is to propose a method to reduce the sensitivity of the estimated omnipolar electrogram (oEGM) with respect to the angle of the propagation wavefront.
Methods: A novel configuration of cliques taking into account all four electrodes of a squared cell is proposed. To test this approach, simulations of HD grids of cardiac activations at different propagation angles, conduction velocities, interelectrode distance and electrogram waveforms are considered.
Results: The proposed approach successfully provided narrower loops (essentially a straight line) of the electrical field described by the bipole pair with respect to the conventional approach. Estimation of the direction of propagation was improved. Additionally, estimated oEGMs presented larger amplitude, and estimations of the local activation times were more accurate.
Conclusions: A novel method to improve the estimation of oEGMs in HD grid of electrodes is proposed. This approach is superior to the existing methods and avoids pitfalls not yet resolved.
Relevance: Robust tools for quantifying the cardiac substrate are crucial to determine with accuracy target ablation sites during an electrophysiological procedure.

1. Introduction

Accurate characterization of the electrophysiologic substrate is crucial in identifying regions responsible for some cardiac arrhythmias and other cardiac disorders such as ventricular tachycardia [1], Brugada Syndrome [2], and atrial fibrillation (AF) [3], among others. In the case of ventricular tachycardia with a reentry mechanism, regions of fibrosis with surviving myocyte bundles create fixed or functional conduction blocks in addition to slow conduction. In this scenario, stable circuits can be mapped with high density mapping catheters and later modeled accordingly. Accurate mapping of the substrate is essential in determining the degree of conduction delay and the critical isthmus. Moreover, remodeling of the myocardium following an infarction contributes to the formation of channels and regions in which conduction time is prolonged, facilitating the initiation of a reentry [4]. In the case of AF, the substrate for AF relates to left atrial (LA) dilation and fibrosis with subsequent LA dysfunction and delay in electromechanical conduction. Regions with anomalous conduction such as fibrotic tissue are associated to arrhythmogenic substrates in AF [5] and, therefore, may become target ablation sites [6]. Indeed, previous studies have shown that areas with fibrosis – detected with late gadolium enhanced magnetic resonance imaging – are correlated to lower voltage EGMs and slower conduction velocity (CV) [7]. Therefore, accurate mapping of these regions would undoubtedly provide important information that can be used for substrate modification during an electrophysiological procedure.

However, despite the importance of quantitative EGM biomarkers – such as amplitude and degree of fractionation – for identifying candidate target ablation sites, discrepancies in the detection of low-voltage regions between different electroanatomic mapping systems as yet remain unresolved [8]. Additionally, accurate detection of local activation times (LATs) is required to quantify parameters related to the propagation of the activation wavefront, such as CV. There are two

* Correspondence to: Bülachstrasse 1C, 8057 Zurich, Switzerland.
E-mail address: sruiperez@berkeley.edu (S. Ruipérez-Campillo).
[1] F. Castells and S. Ruipérez-Campillo have contributed equally, being first authors of this work.

https://doi.org/10.1016/j.compbiomed.2023.106604
Received 17 October 2022; Received in revised form 18 January 2023; Accepted 22 January 2023
Available online 25 January 2023

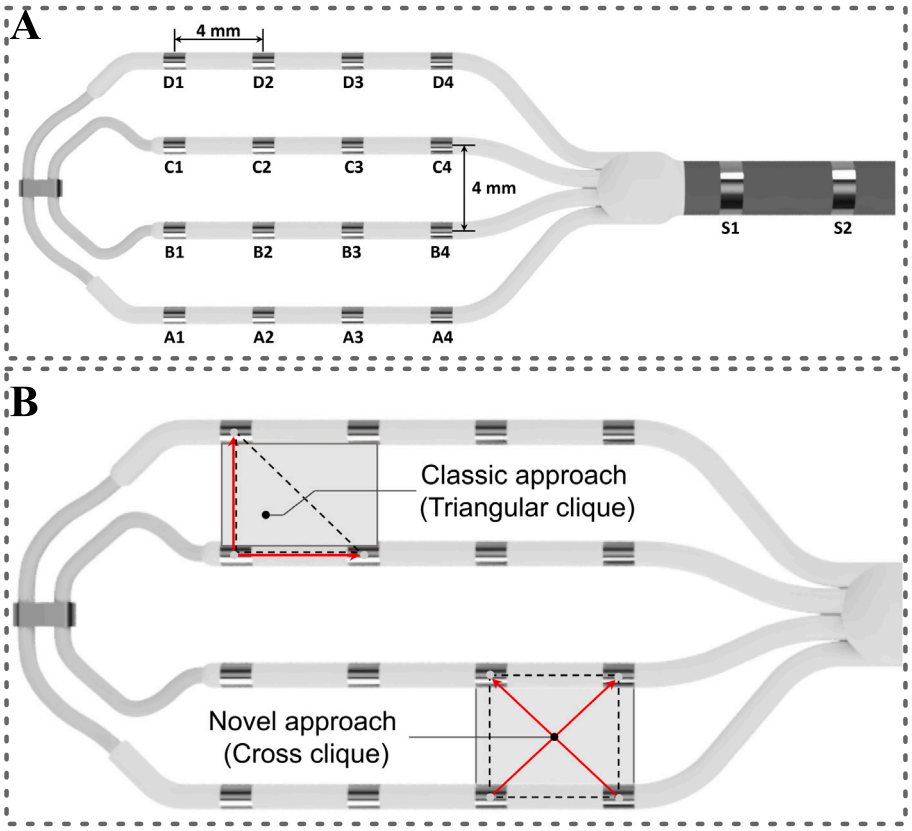

Fig. 1. Representation of the geometry of the Advisor™HD Grid Mapping Catheter (Abbott Laboratories, Illinois, US). **A**: Geometry and position of the electrodes in a model of the device (not to scale, see measuring marks). **B**: Illustration of the classic approach of a triangular clique on one of the four-electrode configurations (upper left) and the novel approach described in this work, that is, the cross clique (lower right).

main modes to obtain intracardiac EGMs. One of which is whereby unipolar EGMs (uEGMs) are recorded from the differential potential between an exploring electrode and a distant electrode. On the other hand, bipolar EGMs (bEGMS) are obtained from the differential potential between a pair of closely spaced electrodes (with interelectrode distance of few millimeters). Whereas uEGMs present some problems related to electric far-field interference [9], bEGMs are sensitive to the orientation of the bipole pair with respect to the direction of the propagation wavefront [10] and catheter contact angle, among other factors [11]. In order to overcome these limitations, an ingenious way to obtain an oriented-independent bEGM from high-density multielectrode arrays – denoted as omnipolar EGM (oEGM) – has been recently proposed [12]. This method, also referred to as orientation-independent sensing (OIS), requires a grid of regularly arranged unipolar electrodes. Using this concept, the Advisor™HD Grid Mapping Catheter (Abbott Laboratories, Illinois, US) was developed [13] for a better characterization of the electrophysiological substrate [14]. This catheter consists of a 4 × 4 grid of unipolar electrodes regularly arranged with an interelectrode distance of 4 mm, which allows a thorough exploration of the local cardiac tissue (see Fig. 1.A) [15]. This catheter has been successfully used for substrate exploration, e.g. for scar detection [16], characterization of conduction gaps [17], atrial disorders such as AF [18] or ventricular tachycardia [19], amongst others.

To estimate an oEGM, at least three unipolar electrodes arranged as the vertices of a triangle are required. The group of electrodes involved to estimate the oEGM has been denoted as a clique [15]. Furthermore, a close proximity between electrodes is required to satisfy the assumption of a locally plane and homogeneous propagation within the clique. Using a configuration based on an isosceles right angled triangle, two orthogonal bEGMs are obtained from the electrodes at the short sides (notice that the unipolar electrode corresponding with the vertex at the right angle is used twice). The representation of the electrical field from a pair of orthogonal bEGMs describes a loop with maximal modulus in the direction of propagation [14]. Subsequently, the oEGM can be computed as the orthogonal transformation that maximizes the amplitude of the activation (i.e. a geometric rotation of the raw data). Accordingly, oEGMs can be regarded as virtual representations of bEGMs as if they were captured from an electrode pair matching the direction of the propagation wavefront. This provides a more meaningful measure of the real amplitude of the activation in comparison to uEGMs and bEGMs, hence, allowing a more robust detection of low-voltage areas [20]. Additionally, it also allows an estimation of the direction of propagation and higher accuracy in the detection of local activation times.

Applying this concept to a cell of 2 × 2 electrodes, 4 triangular cliques can be defined according to the triad of electrodes considered. For each of those cliques, the oEGM can be derived. When extrapolating it to a 4 × 4 grid of unipolar electrodes (i.e. 3 × 3 cells), this technique provides an array of 6 × 6 cliques, with 2 × 2 cliques arranged per cell [21]. Furthermore, the estimation of such a high-density oEGMs matrix allows other measurements such as CV or heterogeneity of the propagation.

Although claimed as an orientation-independent EGM, a recent study has shown significant sensitivity in the reconstruction of the oEGM with respect to the direction of propagation [22]. Additionally, it concluded that the cause for errors in the estimation of oEGMs were temporal misalignments between bipolar activations. This limitation reveals an important research gap regarding the OIS approach, since the electrode configurations and settings under which the orientation independence condition is satisfied remain to be unexplored.

In this study we aim to address that research gap, by evaluating the performance of different clique configurations and interelectrode

distances. For this, we considered the conventional triangular clique employed in clinical practice as well as square and cross-oriented cliques using the four electrodes of a 2 × 2 cell. Whereas the square clique obtains average bipole pairs by averaging the two horizontal and two vertical bipoles of the square, respectively, the cross-oriented clique employs the diagonal bipoles pairs. We hypothesize that misalignments occurring with triangular cliques can be reduced with other clique configurations and hence, providing oEGMs less sensitive to the direction of the propagation wavefront. Additionally, the effect of interelectrode distance is explored. To test our hypothesis, we explored the sensitivity to angle orientation of different clique configurations using controlled simulations. Specifically, we analyzed the dependence of the performance as a function of the following parameters: CV, morphology of the signal, and interelectrode distance.

This manuscript is organized as follows: Section 2 elaborates on the methods, describing the simulations, clique configurations, procedure to estimate the oEGM and the parameters for performance assessment. Section 3 shows an objective comparison of performance using different clique configurations and electrode spacing, which are discussed in-depth in Section 4. Finally, Section 5 concludes this work with the main remarks and outcomes of the study.

2. Methods

The purpose of synthetic signals is to quantify the influence of the angle orientation in the estimation of oEGMs. With that objective, simulated clique activations with known propagation directions and CV are generated. Considering the waveform of real uEGM activations sampled from intracardiac clinical data, we replicated delayed versions according to the direction of the propagation wavefront and the position of each electrode within the multielectrode grid. Fig. 1. A illustrates the multielectrode arrangement, with A-D and 1–4 denoting rows and columns, respectively. Montecarlo simulations were carried out considering randomized propagation angles, CV within physiological range (from 0.5 m/s to 1 m/s) and random selection of atrial uEGMs among 5 different patterns taken from clinical recordings at different atrial sites. Furthermore, we considered different distances from 1 mm to 4 mm, in steps of 1 mm. For each interelectrode distance, 100 simulations were undertaken in accordance with the aforementioned variables.

2.1. Configurations of bEGMs within a clique

Given a cell with 2 × 2 electrodes, up to 6 bEGMs can be computed: the four side bEGMs b_{A2-A1}, b_{B2-B1}, b_{A1-B1} and b_{A2-B2}, plus the diagonal bEGMs b_{A2-B1} and b_{A1-B2}. Being b_x and b_y the bEGMs corresponding to x and y axes, respectively, the conventional triangular clique configurations are defined as [22]:

- Top left triangle: $b_x(t) = b_{B2-B1}(t)$ and $b_y(t) = b_{B1-A1}(t)$
- Top right triangle: $b_x(t) = b_{B2-B1}(t)$ and $b_y(t) = b_{B2-A2}(t)$
- Bottom left triangle: $b_x(t) = b_{A2-A1}(t)$ and $b_y(t) = b_{B1-A1}(t)$ (see Fig. 1.B, Triangular clique)
- Bottom right triangle: $b_x(t) = b_{A2-A1}(t)$ and $b_y(t) = b_{B2-A2}(t)$

Notice that the geometrical center of each of the bEGMs involved in the clique, regardless of the triangle configuration, are coincidental (see geometry in Fig. 1.B, Triangular clique). This is a major drawback when combining EGMs that are not spatially – and hence, neither temporally – aligned. Notice also that, in the case of triangular configurations, there is always an electrode that is used twice (in both horizontal and vertical bEGMs), whereas there is always an electrode that lays unused. Apart from the classical triangular cliques, two alternative configurations that make use of the four electrodes of the square cell can be defined as:

- Square: $b_x(t) = \frac{1}{2}\left(b_{A2-A1}(t) + b_{B2-B1}(t)\right)$ and $b_y(t) = \frac{1}{2}\left(b_{B1-A1}(t) + b_{B2-A2}(t)\right)$
- Cross: $b_{d_1}(t) = b_{B2-A1}(t)$ and $b_{d_2}(t) = b_{B1-A2}(t)$

Notice that the diagonal bipoles of the square cell are utilized for the cross-oriented clique (see Fig. 1.B, Cross clique), which imposes a coincident center for both bipoles. Regardless of the configuration considered, we can define the vector $\mathbf{b}(t)$ containing the orthogonal bipole pair, with $\mathbf{b}(t) = [b_x(t) \quad b_y(t)]^{\mathrm{T}}$. In the case of the cross-oriented configuration, the unique correction left to be done to determine $\mathbf{b}(t)$ is a simple counterclockwise rotation of $\frac{\pi}{4}$rad:

$$\mathbf{b}(t) = \begin{bmatrix} \cos\frac{\pi}{4} & -\sin\frac{\pi}{4} \\ \sin\frac{\pi}{4} & \cos\frac{\pi}{4} \end{bmatrix} \mathbf{d}(t) = \frac{1}{\sqrt{2}} \begin{bmatrix} 1 & -1 \\ 1 & 1 \end{bmatrix} \mathbf{d}(t), \tag{1}$$

where $\mathbf{d}(t) = \left[b_{B2-A1}(t) \quad b_{B1-A2}(t)\right]^{\mathrm{T}}$ is the pair of diagonal bEGMs. Therefore, after this orthogonal transformation, the problem to solve remains the same as using the configurations previously mentioned. Despite the fact that square and cross-oriented cliques arise from different definitions, it can be proven that both yield to an equivalent $\mathbf{b}(t)$ vector up to a scaling factor. By breaking down the notation of bEGMs as uEGMs difference (e.g. $b_{A2-A1}(t) = u_{A2}(t) - u_{A1}(t)$):

$$\begin{aligned} \mathbf{b}_{\mathrm{cross}}(t) &= \frac{1}{\sqrt{2}} \begin{bmatrix} 1 & -1 \\ 1 & 1 \end{bmatrix} \begin{bmatrix} u_{B2}(t) - u_{A1}(t) \\ u_{B1}(t) - u_{A2}(t) \end{bmatrix} \\ &= \frac{1}{\sqrt{2}} \begin{bmatrix} (u_{B2}(t) - u_{B1}(t)) + (u_{A2}(t) - u_{A1}(t)) \\ (u_{B2}(t) - u_{A2}(t)) + (u_{A1}(t) - u_{B1}(t)) \end{bmatrix} = \sqrt{2}\mathbf{b}_{\mathrm{square}}(t) \end{aligned} \tag{2}$$

Accordingly, we will unify both square and cross-oriented configurations and refer to them in the following as the square clique.

2.2. Estimation of oEGMs

When representing the local electrical field in a clique from a pair of orthogonal bEGMs, it describes a loop that points to the direction of propagation. In the case of a plane and homogeneous wavefront – as it should be fulfilled with HD grids –, the loop should become narrow enough to almost fit a straight line. As long as oEGMs are defined as the projections of orthogonal bEGM pairs on the direction of wavefront propagation, this transformation ideally exhibits maximal peak amplitude of the activation. In addition, the projection on a perpendicular axis would provide a residual signal with low amplitude. In accordance with this, the oEGM is computed as the projection that maximizes the ratio of the oEGM peak amplitude to the peak amplitude of the residue:

$$\hat{\theta} = \underset{\theta}{\mathrm{argmax}} \left[\frac{\max\left([\cos\theta \quad -\sin\theta]\,\mathbf{b}(t)\right)}{\max\left|[\sin\theta \quad \cos\theta]\,\mathbf{b}(t)\right|} \right] \tag{3}$$

$$\mathbf{o}(t) = \begin{bmatrix} \cos\hat{\theta} & -\sin\hat{\theta} \\ \sin\hat{\theta} & \cos\hat{\theta} \end{bmatrix} \mathbf{b}(t) \tag{4}$$

where $\mathbf{o}(t) = [o(t) \quad o_{\perp}(t)]$, being $o(t)$ the estimated oEGM and $o_{\perp}(t)$ the residual bipolar signal resulting from the projection on the orthogonal axis to the direction of the propagation wavefront. The direction of the wavefront can be estimated as $\Psi = -\hat{\theta}$.

2.3. Assessment of oEGM estimation

The quality of oEGM estimations from simulations of perfectly plane and homogeneous wavefront propagations will be assessed from the peak amplitudes of the pulses retrieved from vector $\mathbf{o}(t)$: $p_o = \max(o(t))$ and $p_{o_{\perp}} = \max\left(\left|o_{\perp}(t)\right|\right)$, as well as the peak ratio $r = p_o/p_{o_{\perp}}$. In order to assess top performance limits for each configuration, true propagation directions will be employed to compute $\mathbf{o}(t)$. Best fits to the real oEGM would exhibit higher p_o, lower $p_{o_{\perp}}$ and, therefore, higher r values.

With respect to the accuracy in the detection of LATs, these are estimated as the instant at peak amplitude of the oEGM signal [23]. Estimated LATs will then be compared to the ground truth, defined as

the instant at maximum negative slope of the unipolar signal as it passes through the center of the clique.

For the analysis of performance dependence with respect to CV, interelectrode distance and uEGM morphology, a simulation is designed. Regarding morphology, uEGMs with slower/faster deflections (i.e. with smoother or sharper transitions) are considered. For each setting, the consistency of the morphology of the estimated bEGM will be evaluated. This will allow us to assess the robustness of the method as well as its limitations.

2.4. Statistical analysis

Results are provided as mean ± standard deviation (SD), or median and interquartile range (IQR) if required. For data exploration, the distribution of the independent variables was evaluated using Kolmogorov–Smirnov and Mann–Whitney–Wilcoxon tests. A *p-value* of <0.05 was considered statistically significant throughout.

3. Results

Fig. 2 shows bidimensional loops described by orthogonal bEGMs for different bipole configurations, including all triangular orientations and the square clique. For the sake of simplicity, propagation directions $\Psi = 0°, 15°, 30°, 45° and -45°$ were considered. It can be observed that all configurations display a straight line for horizontal propagation (i.e. $\Psi = 0°$ or $\Psi = 180°$). Although not shown, analogous behavior was obtained for exact vertical propagations (i.e. $\Psi = 90°$ and $\Psi = -90°$). For other propagation directions there was at least one configuration that displayed a bidimensional loop.

Widest loops were obtained with triangular configurations at propagation directions perpendicular to the bisector formed by the bEGMs involved. In those cases, the delay between both bipole centers was maximal. As can be observed in Fig. 2, triangular configurations 1 and 4 showed the same pattern although rotated and mirrored. The same occurs with triangular configurations 2 and 3. This can be explained by the fact that the wavefront activates b_x earlier than b_y, or vice versa, depending on the triad of electrodes considered for the clique. As well as this, triangular configurations showed a straight line at propagation directions that matched the bisector of the bEGMs. For example, for $\Psi = 45°$, configurations 2 and 3 displayed a straight line, whereas configurations 1 and 4 displayed a wide loop. Analogous behavior is shown for $\Psi = -45°$, with exchanged roles of the cliques involved. In all cases, the square clique showed consistently narrower loops regardless of the incidence angle. The amplitude of the residual signal at its perpendicular direction was also minimal for the square clique, regardless of the propagation direction (see Fig. 3). Moreover, triangular configurations estimated angle and LATs with higher error and provided oEGMs with lower amplitude and peak ratio.

Fig. 4 shows boxplots comparisons among triangular and square cliques for the following parameters: angle errors, oEGM amplitude, amplitude ratios r and LATs errors. In this figure, an interelectrode distance of 1 mm was considered. In addition, Table 1 shows the numerical results for this and other interelectrode distances. For all parameters, the null hypothesis of the Kolmogorov–Smirnov test of normality was rejected. Accordingly, the Mann–Whitney–Wilcoxon test was performed.

Statistical values for interelectrode distances of 1 mm, 2 mm, 3 mm and 4 mm are shown in Table 1. By increasing the interelectrode distance, the following effects were observed: angle estimation errors increased, oEGM amplitude increased, peak ratios decreased and LAT deviations increased.

Morphologies of bEGMs exhibited dependency on several factors, as depicted in Fig. 5. In panel A, a uEGM with slow deflections (i.e. smoother slopes) was employed. On the other hand, in panel B, a sharper uEGM morphologies was considered.

In each panel, two simulations were carried out. The first simulation consists of a parametric analysis with respect to CV, while keeping the interelectrode distance unchanged. The second simulation is performed with increasing interelectrode distance, while keeping CV constant (1 m/s). Either by decreasing CV or increasing interelectrode distance, the delay between the activations captured by the electrode pair is increased. As can be observed, the larger the delay, the wider the bEGM morphology. In addition, above a certain delay threshold, bEGMs became notched, thus corrupting the bEGM morphology.

For the first simulation and setting the interelectrode distance to 4 mm, bEGMs became notched with CV thresholds of 0.28 m/s and 1 m/s for the smoother and sharper uEGM, respectively. For the second simulation and setting the CV to 1 m/s, notch bEGMs were obtained from interelectrode distance thresholds of 14.4 mm and 3.9 mm for the smoother and sharper uEGM, respectively. These results indicate a higher sensitivity for the uEGM waveforms.

4. Discussion

High-density multielectrode arrays have been widely employed in experimental cardiac electrophysiology, such as patch-clamp experimentation [24], Lagendorff perfused isolated hearts from animal models [25] and in-vivo animals [26]. However, it was not until development of the Advisor™HD Grid Mapping Catheter (Abbott Laboratories, Illinois, US) [15] when became of greater interest in clinical practice. An advantage of this catheter is that it copes with the problem of directional sensitivity of bEGMs. As a result, orientation-independent bipoles are obtained from an algebraic rotation of an orthogonal bipole pair. An oEGM should be regarded as a virtual bipole as if it were captured from a bipole whose electrodes can be dynamically oriented in the direction of the propagation wavefront.

Nevertheless, some problems related to omnipolar catheters still need to be addressed. By definition, geometric centers of the bEGMs involved in a triangular clique are not coincident. This makes the activation wavefront pass through these sites at different time instants, hence causing temporal misalignments among bEGM activations and being a major cause for errors in oEGM estimation. In this work, we demonstrate that incorrect oEGM estimates may occur even with perfectly plane and homogeneous propagation wavefronts. To mitigate this problem, a temporal alignment of activations has already been proposed [22]. However, after temporally shifting bEGM activations, a reliable time reference would no longer be available and thus, hindering reliable LAT detection and CV measurement. Alternatively, we propose to estimate oEGMs from the diagonal bEGMs of the clique, so that both bEGM centers are spatially coincident with the clique center. Therefore, time alignment of activations is no longer required. To the authors' knowledge, this approach has not been proposed yet. With such configuration, thinner loops of the electrical field are described in comparison to triangular cliques. However, amplitude using the square configuration is slightly underestimated. This result is consistent from a theoretical perspective, as it is well-known that the average of delayed pulses results in a wider pulse with lower amplitude [27]. Nevertheless, this is not a real limitation, as it was shown that the equivalent cross-orientation provides larger amplitude oEGMs (scaled by a factor of $\sqrt{2}$). Finally, LAT estimation with the square clique was also more accurate than using triangular configurations. This is an important result, as accuracy in detection of LATs is essential to estimate delays related to wavefront propagation [28]. In general, it can be stated that estimation of oEGMs from squared cliques overperformed triangular configurations.

Effects of interelectrode distance was also explored. By increasing interelectrode distance, loops became wider (lower values between $o(t)$ and $o_\perp(t)$ amplitudes) and errors in the estimation of LATs and propagation directions increased. The unique apparent benefit of increasing interelectrode distance is an increase of the oEGM amplitude. This can be well explained as the amplitude difference of delayed versions

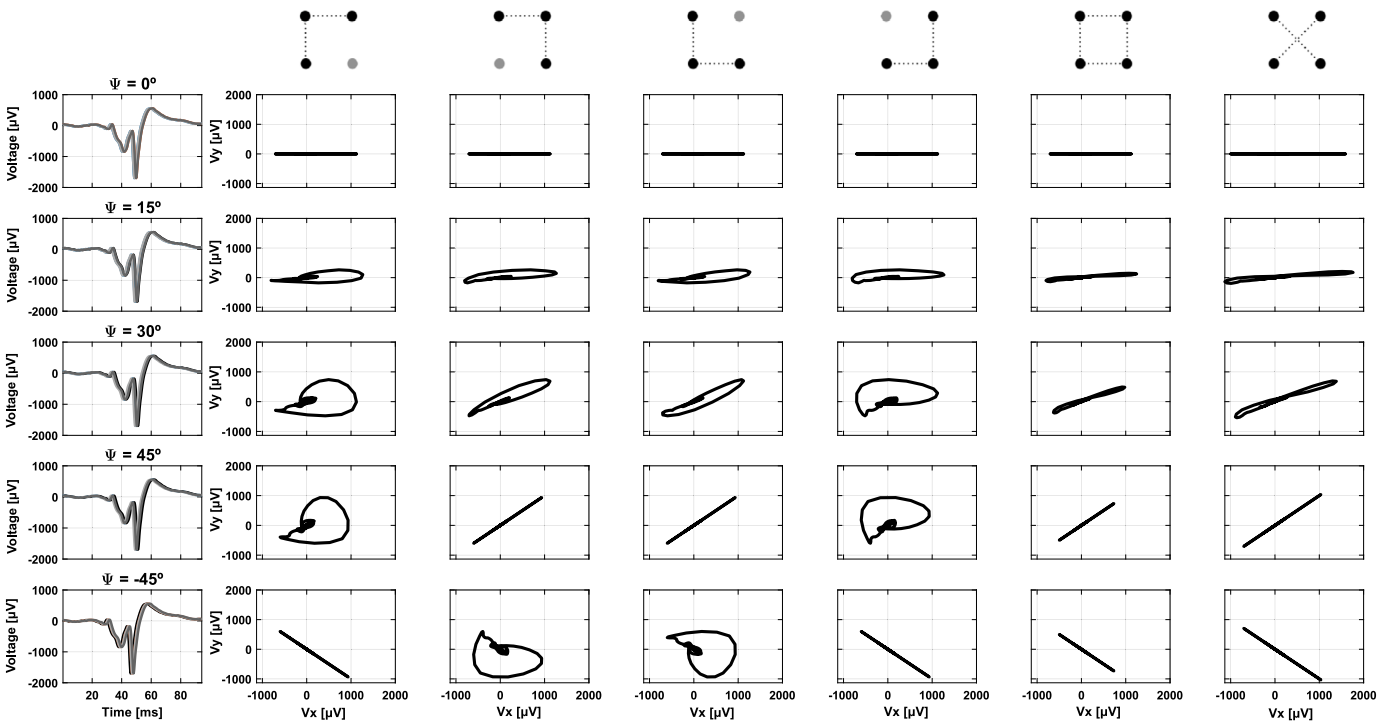

Fig. 2. Bidimensional loops described by orthogonal bEGMs for triangular, square and cross-oriented configurations and propagation directions $\Psi = 0°, 15°, 30°, 45° and -45°$.

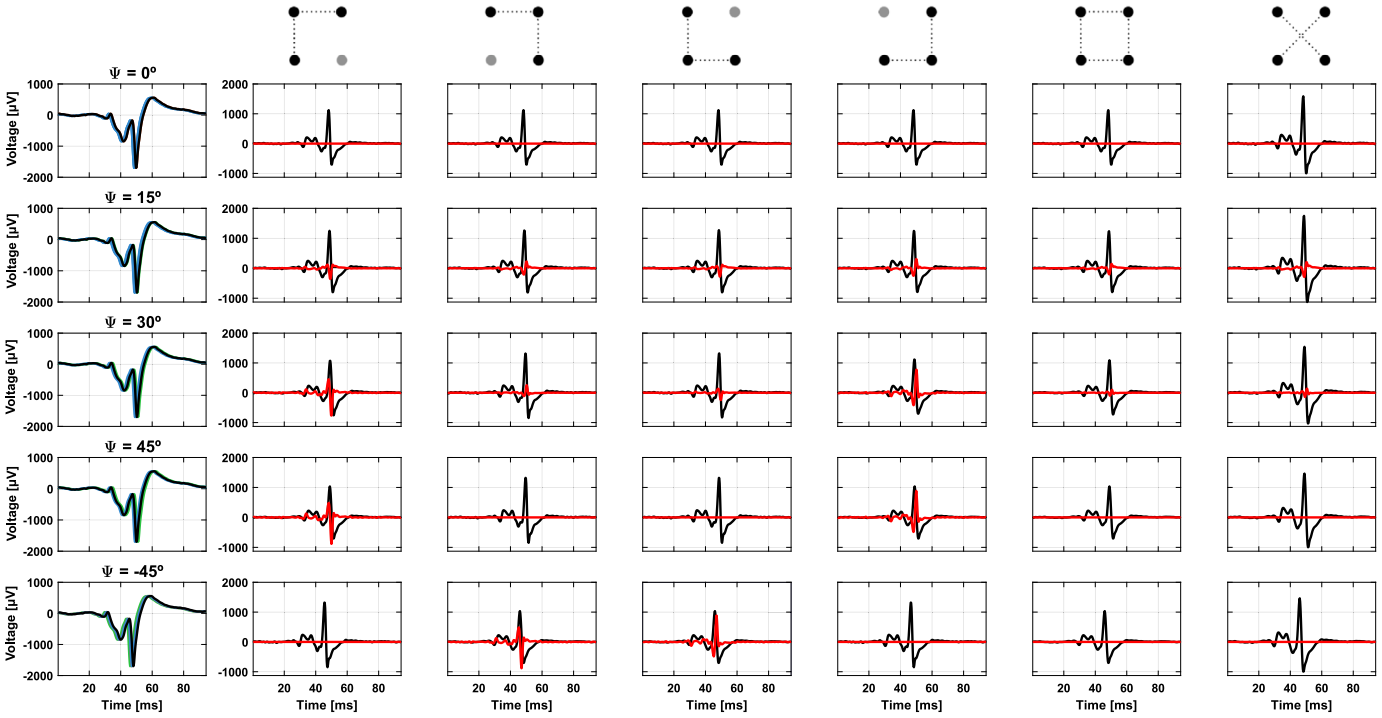

Fig. 3. Omnipolar EGMs (black) and the residual signal $o_{\perp}(t)$ (red) retrieved propagation directions and bipole configurations of Fig. 2.

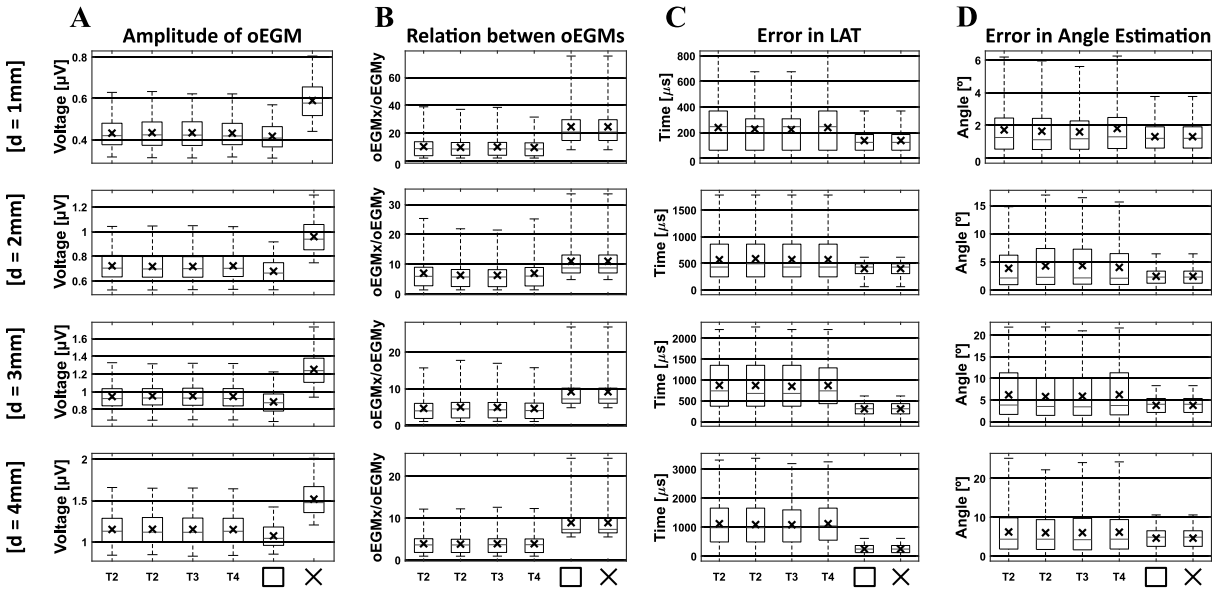

Fig. 4. Boxplot of different variables to compare the bipoles and the triangular and square configuration, namely: **A**: Amplitude oEGM, **B**: Relation between oEGMs, **C**: Error in LAT and **D**: Error in Angle Estimation.

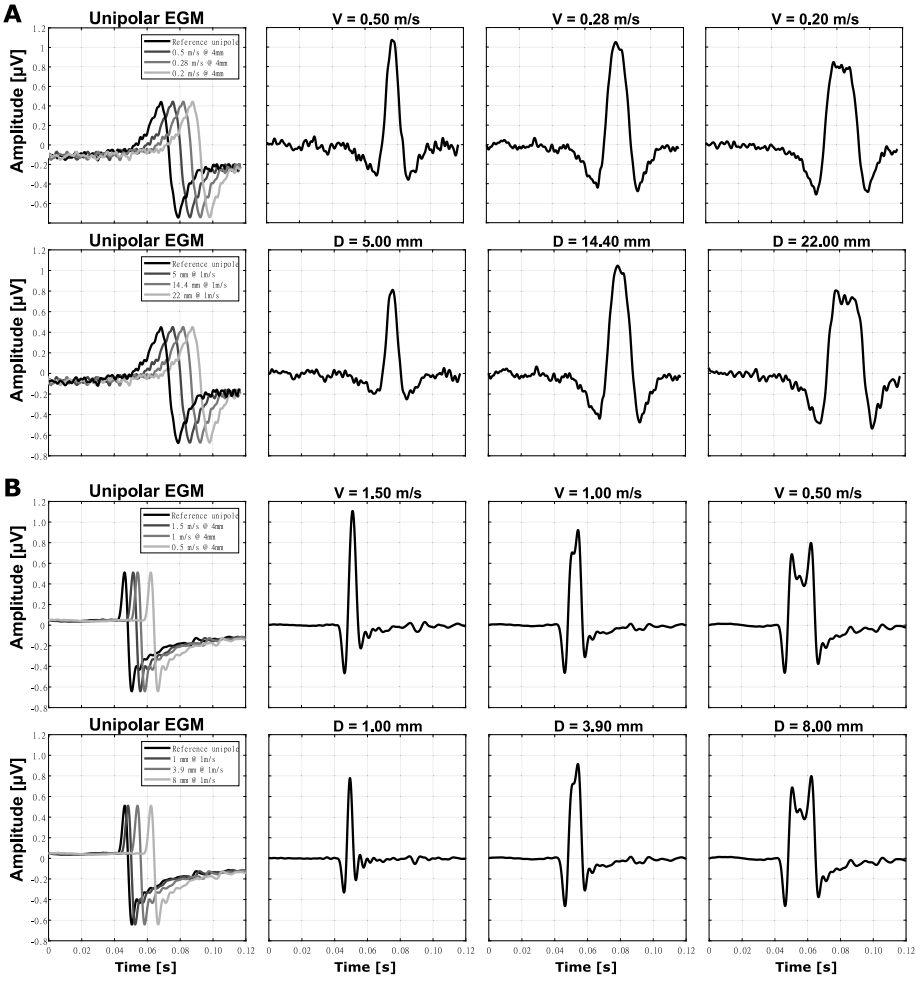

Fig. 5. Illustration of the dependence of the bipolar morphology from with respect to the delay between unipolar signals and uEGM morphologies. Panel **A** and **B** use different uEGM morphologies, with slow and fast deflections, respectively. For rows 1 and 3, an interelectrode distance of 4 mm is fixed. For rows 2 and 4, CV of 1 m/s is fixed. The leftmost panel represents the reference unipole in black, and the three delayed unipoles utilized for the construction of the bipoles, in gray scale. The three rightmost columns represent therefore, the bipoles for each of the parameters according to the first column, being the first of those a valid bipole, the central the illustration of the threshold point at which the notch appears, and the rightmost a non-desired outcome with a clearly visible delay effect.

Table 1
Statistical values of results for simulations.

		Triangle	Square
1 mm	Angle error	1.81 ± 1.56°	1.20 ± 0.83°
	Amplitude	360.17 ± 88.55 μV	345.56 ± 84.45 μV
	Peak ratios[a]	5.98 [2.03… ∞]	10.48 [6.10… ∞]
	LAT error	168.94 ± 148.78 μs	87.18 ± 81.46 μs
2 mm	Angle error	3.37 ± 3.75°	1.94 ± 1.38°
	Amplitude	595.84 ± 139.01 μV	566.04 ± 126.65 μV
	Peak ratios[a]	5.65 [1.40… ∞]	9.01 [4.86… ∞]
	LAT error	437.56 ± 334.48 μs	296.00 ± 152.12 μs
3 mm	Angle error	4.58 ± 4.46°	2.87 ± 1.81°
	Amplitude	976.34 ± 183.33 μV	752.27 ± 162.31 μV
	Peak ratios[a]	5.20 [1.12… ∞]	8.14 [4.84… ∞]
	LAT error	677.13 ± 504.07 μs	365.94 ± 150.67 μs
4 mm	Angle error	5.92 ± 6.02°	3.82 ± 2.20°
	Amplitude	976.34 ± 213.53 μV	911.43 ± 189.64 μV
	Peak ratios[a]	4.76 [0.94… ∞]	7.55 [4.87… ∞]
	LAT error	929.50 ± 651.50 μs	339.88 ± 172.05 μs

[a]Median and range values are shown for this parameter.

of unipolar activations increase with the delay. Another important limitation of increasing interelectrode distance is that a notch may appear at the center of the positive pulse of the bEGM morphology — and thus, the oEGM as well. Indeed, the problem of fractionation in bEGMs computed from spaced uEGMs has been already described [29]. This effect would compromise accuracy in LAT estimation as defined as the instant at which the bEGM amplitude is maximum. Whether this undesirable effect appears or not, not only depends on interelectrode distance, but also on CV and sharpness of unipolar activations. Whereas the interelectrode distance relies on technology, the other constraints depend on the specific patient's electrophysiology. The assessment of slow conduction regions would be specially challenging, e.g. as it occurs with the macroreentrant circuit of atrial flutter [30]. Nevertheless, from an engineering perspective, technology should be designed to work properly regardless of a patient's condition.

The main limitation of the square clique configuration is that activation delays are increased by a factor of $\sqrt{2}$, which are equivalent to an increase of $\sqrt{2}$ of the interelectrode distance, hence resulting in a poorer spatial resolution. As a consequence of that, oEGM estimation can be affected by limitations due to notch deflections in greater extent. Consequently, reducing interelectrode space in future HD catheter designs would be an asset. Additionally, with higher electrode density, the assumption of a plane and homogeneous wavefront propagation would be more easily fulfilled. Nevertheless, some questions ought to be taken into account with reduced interelectrode distances. Firstly, LAT precision under millisecond scale should be required. This could be important to further analyze conduction parameters using the full electrode grid, such as CV and heterogeneity of propagation directions, among others. To achieve such time precision, oversampling of the signals should be considered. Moreover, as lower amplitude oEGMs are obtained, equipment with improved resolution in the acquisition and digitization of the signals could be required to keep similar signal-to-noise ratio levels. Apart from reducing interelectrode distance, other solutions could also be explored, such as staggered multielectrode pattern – to avoid the increasing $\sqrt{2}$ factor aforementioned –, or develop improved signal processing algorithms to enhance oEGM estimation.

5. Conclusions

This paper analyzes limitations of clique configurations for oEGM estimation in orientation-independent sensing from a simulation perspective. The two main conclusions of the study are: firstly, the square clique provides a more robust estimate of omnipolar EGMs. With this approach, pitfalls associated to temporal misalignments are avoided. This approach resolves the still remaining directional sensitivity of these catheters and provides an efficient solution to problems related to the amplitude of bEGMs. Secondly, as long as electrodes are spaced close enough to avoid notch effects in the resulting bEGMs, estimation of wavefront directions and local activation times are consistently improved, which are key factors to obtain high-density CV maps. To better cope with that, interelectrode spacing should be reduced as much as technology allows. Moreover, for multielectrode settings where interelectrode distance is not short enough, the square clique would be less convenient due to a loss of spatial resolution.

Future scope of this work should involve testing in experimental and clinical settings in order to validate and support our conclusions in a more realistic scenario. Studies reporting the limitations and constraints in oEGM estimation are valuable for guiding the design and implementation of future generation catheters and mapping software.

Supplementary material - code

The code written for this manuscript can be found in the following github link: https://github.com/SamuelRuiperezCampillo/F_Castells_S_Ruiperez-Campillo_et_al_CBM_2023_Omnipolar

Declaration of competing interest

The authors declare the following financial interests/personal relationships which may be considered as potential competing interests: Dr. JLM reports receiving speaker fees, honoraria, consultancy, advisory board fees, investigator, committee member, etc. from Medtronic, Microport, Sanofi Aventis, Boston Scientific and Abbott, Dr. RCA reports educational talks for Abbott and Boston scientific. Drs. FC, RC, JM and Mr. SRC and IS report no disclosures.

Acknowledgments

This work was supported by PID2019-109547RB-I00 (National Research Program, Ministerio de Ciencia e Innovación, Spanish Government) and CIacBERCV CB16/11/00486 (Instituto de Salud Carlos III). We would like express our gratitute to the *Rafael del Pino Foundation* and *La Caixa Foundation* for the support and contribution to the academic training of one first author of the manuscript (S. Ruipérez-Campillo).

References

[1] David A. Cesario, Marmar Vaseghi, Noel G. Boyle, Michael C. Fishbein, Miguel Valderrábano, Calambur Narasimhan, Isaac Wiener, Kalyanam Shivkumar, Value of high-density endocardial and epicardial mapping for catheter ablation of hemodynamically unstable ventricular tachycardia, Heart Rhythm 3 (1) (2006) 1–10.

[2] P.D. Lambiase, A.K. Ahmed, E.J. Ciaccio, R. Brugada, E. Lizotte, S. Chaubey, Ron Ben-Simon, A.W. Chow, M.D. Lowe, W.J. McKenna, High-density substrate mapping in brugada syndrome: combined role of conduction and repolarization heterogeneities in arrhythmogenesis, Circulation 120 (2) (2009) 106–117, 1–4.

[3] Thomas Rostock, Martin Rotter, Prashanthan Sanders, Yoshihide Takahashi, Pierre Jaïs, Mélèze Hocini, Li-Fern Hsu, Fréderic Sacher, Jacques Clémenty, Michel Haïssaguerre, High-density activation mapping of fractionated electrograms in the atria of patients with paroxysmal atrial fibrillation, Heart Rhythm 3 (1) (2006) 27–34.

[4] Stephen M. Dillon, Maurits A. Allessie, Philip C. Ursell, Andrew L. Wit, Influences of anisotropic tissue structure on reentrant circuits in the epicardial border zone of subacute canine infarcts, Circ Res 63 (1) (1988) 182–206.

[5] Nassir F. Marrouche, David Wilber, Gerhard Hindricks, Pierre Jais, Nazem Akoum, Francis Marchlinski, Eugene Kholmovski, Nathan Burgon, Nan Hu, Lluis Mont, Thomas Deneke, Mattias Duytschaever, Thomas Neumann, Moussa Mansour, Christian Mahnkopf, Bengt Herweg, Emile Daoud, Erik Wissner, Paul Bansmann, Johannes Brachmann, Association of atrial tissue fibrosis identified by delayed enhancement MRI and atrial fibrillation catheter ablation: the DECAAF study, JAMA 311 (5) (2014) 498.

[6] Dennis H. Lau, Dominik Linz, Ulrich Schotten, Rajiv Mahajan, Prashanthan Sanders, Jonathan M. Kalman, Pathophysiology of paroxysmal and persistent atrial fibrillation: Rotors, foci and fibrosis, Heart Lung Circ. 26 (9) (2017) 887–893.

[7] Gala Caixal, Francisco Alarcón, Till F. Althoff, Marta Nuñez-Garcia, Eva Maria Benito, Roger Borràs, Rosario Jesus Perea, Susana Prat-González, Paz Garre, David Soto-Iglesias, Clara Gunturitz, Jennifer Cozzari, Markus Linhart, Jose Maria Tolosana, Elena Arbelo, Ivo Roca-Luque, Marta Sitges, Eduard Guasch, Lluis Mont, Accuracy of left atrial fibrosis detection with cardiac magnetic resonance: correlation of late gadolinium enhancement with endocardial voltage and conduction velocity, Europace 23 (3) (2021) 380–388.

[8] Kenichi Kaseno, Kanae Hasegawa, Shinsuke Miyazaki, Moe Mukai, Daisetsu Aoyama, Minoru Nodera, Koudai Hirano, Mika Otake, Ryouhei Nomura, Kousuke Miyahara, Rie Ishikawa, Akira Matsui, Junya Yamaguchi, Yuichiro Shiomi, Naoto Tama, Hiroyuki Ikeda, Yoshitomo Fukuoka, Kentaro Ishida, Hiroyasu Uzui, Hiroshi Tada, Discrepancy between CARTO and rhythmia maps for defining the left atrial low-voltage areas in atrial fibrillation ablation, Heart Vessels 36 (7) (2021) 1027–1034.

[9] Piotr Podziemski, Pawel Kuklik, Arne van Hunnik, Stef Zeemering, Bart Maesen, Ulrich Schotten, Far-field effect in unipolar electrograms revisited: High-density mapping of atrial fibrillation in humans, in: Annu Int Conf IEEE Eng Med Biol Soc, Vol. 2015, 2015, pp. 5680–5683.

[10] Stephen Gaeta, Tristram D. Bahnson, Craig Henriquez, Mechanism and magnitude of bipolar electrogram directional sensitivity: Characterizing underlying determinants of bipolar amplitude, Heart Rhythm 17 (5 Pt A) (2020) 777–785.

[11] Minki Hwang, Jaehyuk Kim, Byounghyun Lim, Jun-Seop Song, Boyoung Joung, Eun Bo Shim, Hui-Nam Pak, Multiple factors influence the morphology of the bipolar electrogram: An in silico modeling study, PLoS Comput Biol 15 (4) (2019) e1006765.

[12] Shouvik Haldar, Karl Magtibay, Andreu Porta-Sánchez, Stephane Masse, Nicholas Mitsakakis, Patrick Lai, Mohammed Azam, John Asta, Marjan Kusha, Paul Dorian, Andrew Ha, Vijay Chauhan, Curt Deno, Kumaraswamy Nanthakumar, Resolving bipolar electrogram voltages during atrial fibrillation using omnipolar mapping, Circul.: Arrhythmia Electrophysiol. 10 (2017) e005018.

[13] Don Curtis Deno, et al., Orientation independent sensing, mapping, interface and analysis systems and methods, 2018, WO2018191686.

[14] Karl Magtibay, Andreu Porta-Sánchez, Shouvik K. Haldar, Don Curtis Deno, Stéphane Massé, Kumaraswamy Nanthakumar, Reinserting physiology into cardiac mapping using omnipolar electrograms, Card. Electrophysiol. Clin. 11 (3) (2019) 525–536.

[15] Don Curtis Deno, Ram Balachandran, Dennis Morgan, Faiz Ahmad, Stéphane Massé, Kumaraswamy Nanthakumar, Orientation-independent catheter-based characterization of myocardial activation, IEEE Trans Biomed Eng 64 (5) (2017) 1067–1077.

[16] Masateru Takigawa, Jatin Relan, Takeshi Kitamura, Claire A. Martin, Steven Kim, Ruairidh Martin, Ghassen Cheniti, Konstantinos Vlachos, Grégoire Massoullié, Antonio Frontera, Nathaniel Thompson, Michael Wolf, Felix Bourier, Anna Lam, Josselin Duchateau, Thomas Pambrun, Arnaud Denis, Nicolas Derval, Xavier Pillois, Julie Magat, Jerome Naulin, Mathilde Merle, Florent Collot, Bruno Quesson, Hubert Cochet, Mélèze Hocini, Michel Haïssaguerre, Frederic Sacher, Pierre Jaïs, Impact of spacing and orientation on the scar threshold with a high-density grid catheter, Circ. Arrhythm. Electrophysiol. 12 (9) (2019) e007158.

[17] J.L. Merino, S. Kim, S. Castrejon, J. Relan, M. Sanroman-Junquera, M. Martinez-Cossiani, C. Escobar, A. Carton, Characterization of conduction gaps at the pulmonary vein antra by omnipolar voltage mapping, Europace 23 (Supplement_3) (2021).

[18] Wen-Han Cheng, Li-Wei Lo, Yenn-Jiang Lin, Shih-Lin Chang, Yu-Feng Hu, Fa-Po Chung, Ta-Chuan Tuan, Tze-Fan Chao, Jo-Nan Liao, Ting-Yung Chang, Chin-Yu Lin, Ling Kuo, Shin-Huei Liu, Jennifer Jeanne Vicera, Isaiah C. Lugtu, Steven Kim, Shih-Ann Chen, Identification of circumferential pulmonary vein isolation gaps and critical atrial substrate from HD grid maps in atrial fibrillation patients: Insights from omnipolar technology, Circul.: Arrhythmia Electrophysiol. 15 (1) (2022) e010424.

[19] Andreu Porta-Sánchez, Karl Magtibay, Sachin Nayyar, Abhishek Bhaskaran, Patrick F.H. Lai, Stéphane Massé, Christopher Labos, Beiping Qiang, Rocco Romagnuolo, Hassan Masoudpour, Labonny Biswas, Nilesh Ghugre, Michael Laflamme, Don Curtis Deno, Kumaraswamy Nanthakumar, Omnipolarity applied to equi-spaced electrode array for ventricular tachycardia substrate mapping, Europace 21 (5) (2019) 813–821.

[20] Mathijs van Schie, Rohit Kharbanda, Charlotte Houck, Eva Lanters, Yannick Taverne, Ad Bogers, Natasja Groot, Identification of low-voltage areas: A unipolar, bipolar, and omnipolar perspective, Circul. Arrhythmia Electrophysiol. 14 (2021) 627–637.

[21] Curt Deno, Abhishek Bhaskaran, Dennis Morgan, Fikri Goksu, Katherine Batman, Gregory Olson, Karl Magtibay, Sachin Nayyar, Andreu Porta-Sánchez, Michael Laflamme, Stephane Masse, Prashant Aukhojee, Krishnakumar Nair, Kumaraswamy Nanthakumar, High resolution, live, directional mapping, Heart Rhythm (2020).

[22] Jennifer Riccio, Alejandro Alcaine, Sara Rocher, Laura Martinez-Mateu, Sergio Laranjo, Javier Saiz, Pablo Laguna, Juan Pablo Martínez, Characterization of atrial propagation patterns and fibrotic substrate with a modified omnipolar electrogram strategy in multi-electrode arrays, Front. Physiol. 12 (2021).

[23] T. Paul, J.P. Moak, C. Morris, A. Garson Jr., Epicardial mapping: how to measure local activation? Pacing Clin. Electrophysiol. 13 (3) (1990) 285–292.

[24] Kurt Pfannkuche, Huamin Liang, Tobias Hannes, Jiaoya Xi, Azra Fatima, Filomain Nguemo, Matthias Matzkies, Marius Wernig, Rudolf Jaenisch, Frank Pillekamp, Marcel Halbach, Heribert Schunkert, Tomo Sarić, Juergen Hescheler, Michael Reppel, Cardiac myocytes derived from murine reprogrammed fibroblasts: intact hormonal regulation, cardiac ion channel expression and development of contractility, Cell Physiol Biochem 24 (1–2) (2009) 73–86.

[25] Francisco J. Chorro, Francisca Pelechano, Isabel Trapero, Xavier Ibañez-Catalá, Luis Such-Miquel, Alvaro Tormos, Juan Guerrero, Joaquín Cánoves, Luis Mainar, José Millet, Antonio Alberola, Luis Such, Modifications in ventricular fibrillation and capture capacity induced by a linear radiofrequency lesion, Rev. Esp. Cardiol. (Engl. Ed.) 65 (2) (2012) 143–151.

[26] Jens Eckstein, Stef Zeemering, Dominik Linz, Bart Maesen, Sander Verheule, Arne van Hunnik, Harry Crijns, Maurits A. Allessie, Ulrich Schotten, Transmural conduction is the predominant mechanism of breakthrough during atrial fibrillation: evidence from simultaneous endo-epicardial high-density activation mapping, Circ. Arrhythm. Electrophysiol. 6 (2) (2013) 334–341.

[27] Leif Sornmo, Pablo Laguna, Bioelectrical Signal Processing in Cardiac and Neurological Applications, in: Biomedical Engineering, Academic Press, San Diego, CA, 2005.

[28] Raquel Cervigón, Javier Moreno, José Millet, Julián Pérez-Villacastín, Francisco Castells, Propofol effects on atrial fibrillation wavefront delays, IEEE Trans Biomed Eng 57 (8) (2010) 1877–1885.

[29] Lisette J.M.E. van der Does, Natasja M.S. de Groot, Inhomogeneity and complexity in defining fractionated electrograms, Heart Rhythm 14 (4) (2017) 616–624.

[30] Samuel Ruipérez-Campillo, Sergio Castrejón, Marcel Martínez, Raquel Cervigón, Olivier Meste, José Luis Merino, José Millet, Francisco Castells, Non-invasive characterisation of macroreentrant atrial tachycardia types from a vectorcardiographic approach with the slow conduction region as a cornerstone, Comput Methods Programs Biomed 200 (2021) 105932.